Volume 8
Number 19
7 October 2020
Pages 5221-5506

Biomaterials Science

rsc.li/biomaterials-science

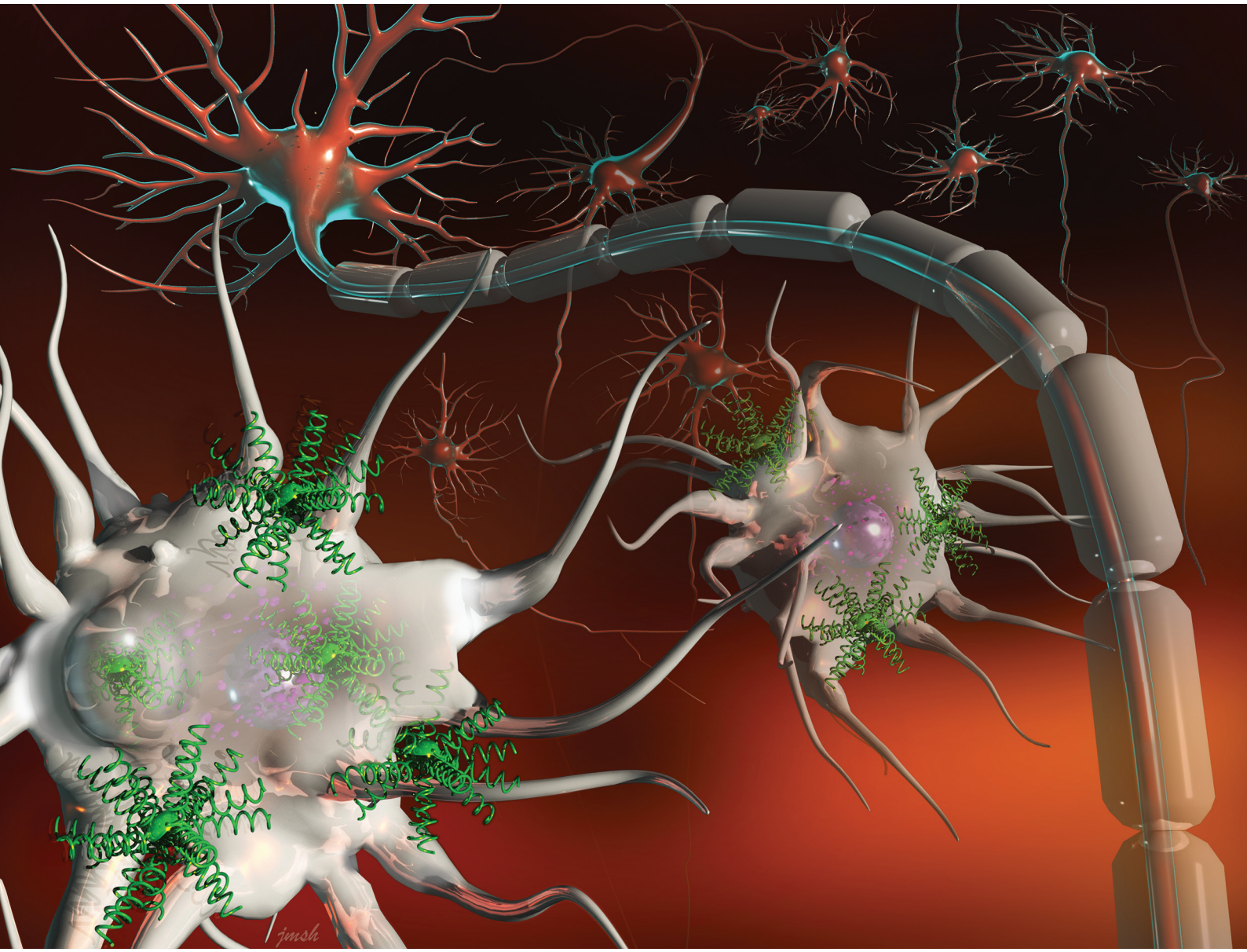

ISSN 2047-4849

ROYAL SOCIETY OF CHEMISTRY

PAPER

Jianjun Cheng, Makoto Inoue *et al.*
Induction of a higher-ordered architecture in glatiramer acetate improves its biological efficiency in an animal model of multiple sclerosis

European Society for Biomaterials

Biomaterials Science

ROYAL SOCIETY OF CHEMISTRY

PAPER

View Article Online
View Journal | View Issue

Cite this: *Biomater. Sci.*, 2020, **8**, 5271

Induction of a higher-ordered architecture in glatiramer acetate improves its biological efficiency in an animal model of multiple sclerosis†

Ziyuan Song, ‡[a,b] Yee Ming Khaw, ‡[a,c] Lazaro A. Pacheco, [b] Kuan-Ying Tseng,[b] Zhengzhong Tan, [b] Kaimin Cai, [b] Ettigounder Ponnusamy,[d] Jianjun Cheng *[b] and Makoto Inoue *[a,c]

Glatiramer acetate (GA), a linear random copolypeptide, is a first-line treatment for multiple sclerosis (MS). A major concern, however, is that GA treatment is associated with adverse effects and poor patient adherence due to the need for frequent injections. Here we describe improved performance of the polymeric drug, even at low doses with less-frequent injections, through the modification of its architecture into a star-shaped GA (sGA). In a sGA, multiple GAs are covalently linked onto a core, which greatly changes their properties such as molecular weight, size, and shape. The spherical sGA is retained longer in the body after intraperitoneal injection, and is more readily internalized by RAW 264.7 macrophage cells and bone marrow-derived dendritic cells than GA. In C57BL/6 mice induced with experimental autoimmune encephalitis, a mouse model for MS, sGA treatment exerts disease amelioration effect that is significantly better than that of GA despite a lower dose and less frequent injection. Moreover, spinal cord pathologies of demyelination and leukocyte infiltration are dramatically less pronounced in the sGA treatment condition compared to the GA treatment condition. Thus, we propose that sGA with a higher-ordered architecture offers an attractive and potentially viable treatment option for MS patients.

Received 11th June 2020,
Accepted 29th July 2020

DOI: 10.1039/d0bm00957a

rsc.li/biomaterials-science

1. Introduction

Multiple sclerosis (MS) is a debilitating disease characterized by inflammation of the central nervous system (CNS) that affects more than 2 million people worldwide.[1–4] Several therapies developed and approved to treat MS in the last three decades have significantly improved the quality of life for patients with MS.[5] Among these therapies, glatiramer acetate (GA) is a major first-line treatment, mainly due to its excellent safety profile.[6] GA is a mixture of random copolypeptides consisting of four amino acids (*i.e.*, alanine, lysine, glutamic acid, and tyrosine),[6] prepared by ring-opening polymerization of the corresponding amino acid *N*-carboxyanhydrides (NCAs) followed by side-chain deprotection.[7,8] Although the detailed mechanism is not well understood,[9] GA significantly reduces relapse rate and the appearance of lesions by magnetic resonance imaging (MRI) in MS patients compared with placebos.[10–13] Severe adverse effects are rarely observed with GA treatment, allowing its widespread use in MS treatment.[1,2,5,14] In fact, GA is the only MS therapy that is safe to use during pregnancy.[2,15]

Despite the broad use of GA in MS treatment, GA use is limited by tolerability issues due to the need for frequent injections. The first approved GA treatment requires daily administration, resulting in injection-related adverse effects such as injection-site swelling and injection-site pain.[11,13] Administration of GA with lower frequency (three times weekly) and higher dosage showed higher patient satisfaction and adherence compared with daily subcutaneous (s.c.) administration with similar clinical effectiveness.[14,16,17] Nevertheless, the use of a large amount of GA is still a concern due to its high cost.[6] Additionally, GA is only considered a moderately effective treatment, and is replaced by more effective therapies upon new relapses and lesions.[2] Therefore, further improving the efficacy and tolerability of GA-related drugs is of great interest.

The need for frequent injection of GA is presumably related to its fast degradation and clearance. Previous studies indicated rapid hydrolysis of most GA molecules into amino acids

[a]*Department of Comparative Biosciences, University of Illinois at Urbana-Champaign, Urbana, Illinois 61801, USA. E-mail: makotoi@illinois.edu*
[b]*Department of Materials Science and Engineering, University of Illinois at Urbana-Champaign, Urbana, Illinois 61801, USA. E-mail: jianjunc@illinois.edu*
[c]*University of Illinois at Urbana-Champaign, Neuroscience Program, 405 North Matthews Avenue, Urbana, Illinois 61801, USA*
[d]*MilliporeSigma, 545 South Ewing, St. Louis, Missouri 63103, USA*
†Electronic supplementary information (ESI) available. See DOI: 10.1039/d0bm00957a
‡These authors contributed equally to this work.

and oligopeptides at the injection site within 1 h after injection.[18,19] Like other engineered polypeptides,[20] GA has its own intrinsic immunogenicity that allows it to potently interact with immune cells and can be modified by altering polymer charge, shape, or chemical functionality.[21] Therefore, we reasoned that changing the structure of GA may alter its degradation and release profiles, thus achieving good efficacy while maintaining low-dose and less-frequent injections. Furthermore, modification of GA dimensionality and density of its functional groups may enhance its effect on immune cells by improving its ability to bind cell surface molecules and/or causing greater internalization capacity. Thus, a GA derivative with a higher-ordered architecture may serve as a promising therapeutic candidate since branched polymers have enhanced immunomodulatory effects attributed to their well-defined three-dimensional structures, controlled size, and high density of surface functionality.[22] Additionally, synthetic polypeptides with complex architectures have shown enhanced biomedical performance in other areas, including drug delivery and gene delivery, compared with their linear analogues.[23–27]

In the article, we reported that star-shaped GA (sGA) exhibited much better performance than linear GA in treatment of experimental autoimmune encephalomyelitis (EAE), a mouse model of MS. Prolonged drug retention and faster uptake by antigen-presenting cells (APCs) were observed with sGA, which is attributed to its spherical structure and larger size. Even at a lower dosage with a single injection, sGA suppressed motor dysfunction and CNS demyelination in EAE mice. We believe this work provides a new strategy to improve GA treatment through structural modification of the polymeric drug, which may inspire the development of new GA therapies with fewer injections and better patient adherence.

2. Materials and methods

2.1 Materials, cells, and animals

All chemicals were purchased from MilliporeSigma (St Louis, MO, USA) unless otherwise specified. Amino acids were purchased from Chem-Impex International Inc. (Wood Dale, IL, USA). Dialysis membrane with a molecular weight cut-off of 1 kDa was purchased from Repligen Corporation (Waltham, MA, USA). Heat-killed *Mycobacterium tuberculosis* (Mtb, DF3114-33-8), RPMI 1640 (11-875-093), and penicillin–streptomycin solution (SV30010) were purchased from Fisher Scientific (Pittsburgh, PA, USA). Myelin oligodendrocyte glycoprotein (35–55) peptide (MOG_{35-55}) was purchased from United Biosystems Inc. (Herndon, VA, USA). Pertussis toxin was purchased from List Biological Laboratories, Inc. (Campbell, CA, USA). Fetal bovine serum (FBS) was purchased from Gemini Bio (West Sacramento, CA, USA). Recombinant mouse GM-CSF (carrier-free) was purchased from Biolegend (San Diego, CA, USA). Goat anti-rat IgG (H + L) secondary antibody (Alexa Fluor 555) and ProLong Gold antifade mountant were purchased from Invitrogen (Carlsbad, CA, USA). CD4 rat anti-mouse antibody (Clone: GK1.5) was purchased from R&D Systems, Inc. (Minneapolis, MN, USA). FITC anti-mouse/human CD11b antibody (Clone: M1/70) was purchased from Biolegend (San Diego, CA).

Anhydrous tetrahydrofuran (THF) and hexane were dried by a column packed with alumina. Anhydrous *N*,*N*-dimethylformamide (DMF) were treated with polymer-bound isocyanates (MilliporeSigma, St Louis, MO, USA) to remove any amine residues. Anhydrous dichloromethane (DCM) were stored over 3 Å molecular sieves in a freezer. The *N*-carboxyanhydride (NCA) monomers, including γ-benzyl-L-glutamate NCA (BLG-NCA),[28] N^{ϵ}-benzyloxycarbonyl-L-lysine NCA (ZLL-NCA),[29] and L-alanine-NCA (Ala-NCA),[30] were synthesized according to previously reported procedures. RAW 264.7 cells were purchased from American Type Culture Collection (Manassas, VA, USA). C57BL/6 mice were purchased from The Jackson Laboratory (Bar Harbor, ME, USA). Healthy mice (6–8 weeks) were randomly selected and used in this study. All mice were group-housed (3–5 mice per cage) in a specific pathogen-free facility with a 12 h light–dark cycle and were fed regular chow *ad libitum*. This study was approved by the University of Illinois at Urbana-Champaign Institutional Animal Care and Use Committee (protocol no. 19171).

2.2 Instrumentation

Proton nuclear magnetic resonance (NMR) spectra were recorded on a Varian U500 or VXR500 spectrometer in the NMR laboratory, University of Illinois. Chemical shifts were reported in ppm and referenced to the residual protons in the deuterated solvents. MestReNova software (version 12.0.3, Mestrelab Research, Escondido, CA, USA) was used for all NMR analysis. Gel permeation chromatography (GPC) experiments were performed on a system equipped with an isocratic pump (1260 Infinity II, Agilent, Santa Clara, CA, USA), a multi-angle static light scattering (MALS) detector (DAWN HELEOS-II, Wyatt Technology, Santa Barbara, CA, USA), and a differential refractometer (dRI) detector (Optilab T-rEX, Wyatt Technology, Santa Barbara, CA, USA). The detection wavelength of HELEOS was set at 658 nm. Separations were performed using serially connected size exclusion columns (three PLgel MIXED-B columns, 10 μm, 7.5 × 300 mm, Agilent, Santa Clara, CA, USA) at 40 °C using DMF containing 0.1 mol L^{-1} LiBr as the mobile phase. The MALS detector was calibrated using pure toluene and can be used for the determination of the absolute molecular weights (MWs). The MWs of polymers were determined based on the d*n*/d*c* value of each polymer sample calculated offline by using the internal calibration system processed by the ASTRA 7 software (version 7.1.3.15, Wyatt Technology, Santa Barbara, CA, USA). Fourier transform infrared (FTIR) were recorded on a Perkin Elmer 100 serial FTIR spectrophotometer (PerkinElmer, Santa Clara, CA, USA) calibrated with polystyrene film. Fluorescent spectra were recorded on a Perkin Elmer LS 55 fluorescence spectrometer (PerkinElmer, Santa Clara, CA, USA). Circular dichroism (CD) measurements were carried out on a JASCO J-815 CD spectrometer (JASCO, Easton, MD, USA). The mean residue molar

ellipticity of each polypeptide was calculated on the basis of the measured apparent ellipticity following the literature-reported formulas: ellipticity ([θ] in deg cm^2 dmol^{-1}) = (millidegrees × mean residue weight)/(path length in millimetres × concentration of polypeptide in mg mL^{-1}).[31,32] Dynamic light scattering (DLS) was performed on Zetasizer Nano (Malvern, Westborough, MA, USA). Fluorescence readings of dye-labelled polypeptides were obtained from a Synergy Neo2 microplate reader (BioTek, Winooski, VT, USA). Confocal images were collected from a Nikon A1R confocal laser microscope system (Melville, NY, USA).

2.3 Synthesis of *O*-benzyloxycarbonyl-L-tyrosine NCA (BLT-NCA)

In a flame-dried, 250 mL Schlenk flask charged with a stir bar, *O*-benzyloxycarbonyl-L-tyrosine (300 mg, 0.95 mmol) was added and dried under vacuum for 2 h. Anhydrous THF (30 mL) was then added into the flask, which was then cooled down to 0 °C in an ice bath. The toluene solution of phosgene (15 wt%, 0.8 mL, 1.14 mmol, 1.2 equiv.) was added into the mixture and stirred at 50 °C for 2 h. (**Caution!** Phosgene is extremely toxic and should be handled with care. All glasswares, needles, and syringes with phosgene solution need to be neutralized with saturated aqueous solution of sodium bicarbonate.) After the removal of excessive phosgene and solvent under vacuum, the product BLT-NCA was purified through silica column chromatography (eluent: anhydrous hexane to anhydrous ethyl acetate/hexane, 8 : 2, v/v). Pure BLT-NCA was isolated as white viscous solid (yield: 53%). ^{1}H NMR ($CDCl_3$, δ, 500 MHz): 7.40 (m, 5H), 7.11 (d, J = 8.50 Hz, 2H), 6.96 (d, J = 8.61 Hz, 2H), 5.43 (s, 1H), 5.06 (s, 2H), 4.48 (dd, J = 8.72 and 4.01 Hz, 1H), 3.28 (dd, J = 8.72 and 4.01 Hz, 1H), 2.92 (dd, J = 8.72 and 4.01 Hz, 1H). ^{13}C NMR ($CDCl_3$, δ, 125 MHz): 168.7, 153.7, 151.6, 150.9, 134.7, 132.1, 130.5, 129.0, 128.9, 128.7, 122.0, 70.7, 58.9, 37.4.

2.4 Synthesis of GA and sGA

In a glovebox, Ala-NCA (23.0 mg, 0.20 mmol), BLG-NCA (17.5 mg, 0.066 mmol), ZLL-NCA (49.0 mg, 0.16 mmol), and BLT-NCA (15.2 mg, 0.044 mmol) were dissolved in anhydrous DMF and mixed, followed by addition of a DMF solution of *n*-hexylamine (0.1 M, 226 μL). The resulting mixture was stirred at room temperature for 24 h, and FTIR analysis indicated >99% conversion of NCA monomers. The precursor of GA with protected side chains was purified by precipitation in hexane/ether (1 : 1, v/v) and isolated as a viscous solid (yield: 72–82%). The precursor of sGA bearing protected side chains was synthesized in a similar manner but using DCM as the solvent and poly(amidoamine) (PAMAM, generation 3.0) as the macroinitiator.

The precursors of GA and sGA were deprotected with HBr to obtain the final polypeptides. Typically, the protected polymer (25 mg, 0.08 mmol of benzyl-protected side chains) was dissolved in trifluoroacetic acid (TFA) at 0 °C, into which an acetic acid solution of HBr (33 wt%, 146 μL, 0.8 mmol, 10 equiv.) was added. The resulting mixture was stirred at 0 °C for 1 h. Yellowish precipitates were observed, indicating successful deprotection. The deprotected polymer was isolated by precipitation in hexane/ether (1 : 1, v/v), and further purified by dialysis against an aqueous solution of sodium acetate (0.1 M) followed by distilled water. The final polymer was obtained as a white powder after lyophilisation (yield: 65–77%).

Cyanine5 (Cy5)-labelled GA and sGA were prepared by mixing an aqueous solution of the corresponding polypeptides (1 mg mL^{-1}) with a DMSO solution of *N*-hydroxysuccinimide (NHS) ester of Cy5 (1 mg mL^{-1}, 0.45 or 1% of lysine residues). The feeding ratio of dyes varied between GA and sGA to ensure similar fluorescence intensity of the final polypeptides, since GA and sGA have different labelling efficiencies. The reaction mixture was left stirring at room temperature overnight and then purified by dialysis against an aqueous solution of sodium acetate (0.1 M) followed by distilled water.

2.5 EAE induction and pharmaceutical treatment

To induce EAE disease, C57BL/6 male mice (6–8 weeks) received s.c. injections of complete Freund's adjuvant (CFA) containing Mtb (200 μg) and MOG_{35-55} (100 μg) at 0 days post immunization (dpi). Pertussis toxin (200 ng per mouse) was administered through intraperitoneal (i.p.) injection at 0 and 2 dpi. GA or sGA (1 mg kg^{-1}, 10 mg kg^{-1}, or 100 mg kg^{-1}) were administered through i.p. injection at 2 dpi (one-time-dosing) or 2 and 5 dpi (two-time-dosing) (n = 4 to 8). Clinical signs of EAE were scored daily for 27 days in a blinded fashion as follows: 0.5, partial tail limpness; 1, tail limpness; 1.5, reversible impaired righting reflex; 2, impaired righting reflex; 2.5, paralysis of one hindlimb; 3, paralysis of both hindlimbs; 3.5, paralysis of both hindlimbs and one forelimb; 4, hindlimb and forelimb paralysis; and 5, death. Water gel and powdered food were provided when the score reached 2 to avoid body weight reduction due to the inability to reach food and water. Disease scoring was performed at midday (during the light cycle). The area under the curve (AUC) was calculated for each animal with respect to behavioural scores from 0 to 27 dpi.

2.6 Pharmacokinetics

C57BL/6 mice (6–8 weeks) were i.p. injected with Cy5-labelled GA or sGA (n = 5). At selected time points (0.5, 1, 2, 4, and 8 h), blood (20 μL) was collected from the submandibular vein (cheek punch), mixed with red blood cell (RBC) lysis buffer (2×, 20 μL), and stored at 4 °C in the dark. The fluorescence readings were collected from the microplate reader (λ_{ex} = 646 nm, λ_{em} = 664 nm) and the concentration of polypeptides was determined through comparison of a standard curve.

2.7 Preparation and treatment of mouse bone marrow-derived dendritic cells (BMDCs)

The tibia, femur, radius, and ulna were removed from male C57BL/6 mice, washed with 70% ethanol, and both ends were cut. Marrow was flushed with PBS containing 2% FBS using a needle (27G). Bone marrow cells were then pelleted by centrifugation (1500 rpm for 5 min) and re-suspended in complete RPMI media supplemented with 10% FBS, penicillin–strepto-

mycin (1×) and glutamine (1×). On day 0, cells were seeded in 6-well plates with RPMI (5 mL, ~2×10^6 cells per well) containing rGM-CSF (20 ng mL^{-1}). On day 3, half of the culture supernatant from each well was removed and fresh complete RPMI media with rGM-CSF was added. On day 7, cells were collected, pelleted by centrifugation, and re-suspended in fresh complete RPMI media.

2.8 Confocal quantitation of sGA uptake by APCs *in vitro*

RAW 264.7 cells (5×10^4 cells per well) were cultured on cover slips in 24-well plates in complete RPMI medium for 24 h. Cy5-labelled GA or sGA was added ($n = 3$) to cultured cells and incubated for 5, 30, and 60 min at 37 °C with carbon dioxide circulation (5%) in a sterile incubator. Cells were washed and fixed with 4% paraformaldehyde and cell membranes were stained with FITC-CD11b antibody. Coverslips were mounted on glass slides with Prolong Gold and stored at 4 °C until image acquisition on a confocal scanning microscope (20× magnification). The integrated fluorescence density of Cy5 channel was quantified using the ImageJ, which was normalized through the cell numbers from the FITC channel. Internalization into BMDCs was quantified in a similar way after 30 min incubation.

2.9 CD4 immunohistochemistry

Spinal cords were harvested from PBS-perfused and 4% paraformaldehyde-fixed mice at EAE 28 dpi. Spinal cords were post-fixed with 4% paraformaldehyde overnight and then cryoprotected by immersing in a sucrose solution (30%) for 24 h. Samples were frozen in optimum cutting temperature compound (OCT) and stored at −80 °C until cryostat sectioning. Transverse sections (30 μm) of spinal cords were mounted on poly(L-lysine) coated glass slides. Mounted samples were permeabilized with Triton-X (0.05%) for 15 min at room temperature, blocked with bovine serum albumin (2%) for 2 h at room temperature, and incubated overnight at 4 °C with rat CD4 primary antibody followed by goat anti-rat Alexa Fluor 555 secondary antibody for 2 h at room temperature. Labelled samples were dried, covered with Prolong Gold mount, and sealed with a coverslip. Ventral median fissure of lumbar spinal cord (3 images per mouse) were visualized using a confocal scanning microscope (20× magnification). The $CD4^+$ T cell count was normalized by spinal cord area (in pixels) using the ImageJ trace and ROI manager function.

2.10 Luxol fast blue (LFB) staining

Transverse sections (30 μm) of OCT gel-embedded spinal cords from mice at 28 dpi were used for LFB staining. Sections were mounted on poly(L-lysine) coated glass slides and left to dry overnight. Mounted samples were dehydrated with 95% ethyl alcohol, incubated in 1 : 1 ethanol/chloroform for 5 minutes, and washed with 95% ethyl alcohol. Mounted samples were then incubated in LFB solution (0.1%) in a 60 °C water bath for 4 h. Excess dye solution was washed away by 95% ethanol, followed by an aqueous solution of Li_2CO_3 (0.05%), 70% ethanol, and distilled water until a sharp contrast between grey and white matter became apparent. After samples were dried, a coverslip was applied using resinous medium. Ventral mid-sections of halved spinal cords (6 images per mouse) were visualized using a brightfield microscope (4× magnification). The area of demyelination (%) was quantified through the ratio of "area of demyelination" to "total area of white matter". Images were converted to 8-bit grey scale in the ImageJ, and the white matter regions of spinal cord half slices were traced to obtain the "total area of white matter". A constant threshold was applied to reveal demyelination lesions to quantitate the "area of demyelination".

2.11 Statistical analysis

All animal and cell studies were statistically analysed using two-tailed unpaired Student's *t*-test. $*p < 0.05$ was considered to be the significant cut-off *p*-value.

3. Results

3.1 Synthesis and characterization of sGA

Polymers with higher-ordered architectures, including brush-like polymers, star-shaped polymers, and other branched polymers, have received increasing attention in recent years due to their unique physiochemical properties and great potential in biomedical applications.[33–35] Similar to the preparation of GA, sGA was synthesized by ring-opening polymerization of four different NCAs followed by side-chain deprotections, using a multiamine PAMAM macroinitiator instead (Scheme 1A). Each PAMAM macroinitiator contains 32 primary amine groups, generating a three-dimensional, spherical, and star-shaped polypeptide, which has a significantly different shape and size from that of the one-dimensional and linear GA (Scheme 1B). To test the preparation of the branched polymer, PAMAM-initiated polymerization of a model monomer, BLG-NCA, was first tested in DMF, the conventional solvent for polypeptide synthesis. Polymerization took overnight to reach >95% monomer conversion, where a significant amount of low-MW species were observed on the GPC-dRI trace (Fig. S1†). We reasoned that the formation of low-MW species originated from side-reactions (*i.e.*, chain-transfer reaction) that occurred due to the slow polymerization of NCAs in DMF, generating linear contaminates.

The recent advances in accelerated polymerization of NCAs provided a powerful strategy to outpace various side reactions during polypeptide synthesis, generating well-defined polypeptide materials.[23,36,37] Therefore, we tested the polymerization of BLG-NCA in DCM with PAMAM as a macroinitiator, which resulted in a monomodal molecular-weight distribution (MWD) with no obvious low-MW species (Fig. S1†), indicating negligible side reactions, consistent with previous studies.[38] Thus, sGA was synthesized by mixing four NCA monomers in DCM, which was polymerized with the addition of a DCM solution of PAMAM. With the accelerated polymerization rate, all NCA monomers were consumed within 2 h, as evidenced by FTIR. As a control, GA was prepared similarly in DMF over-

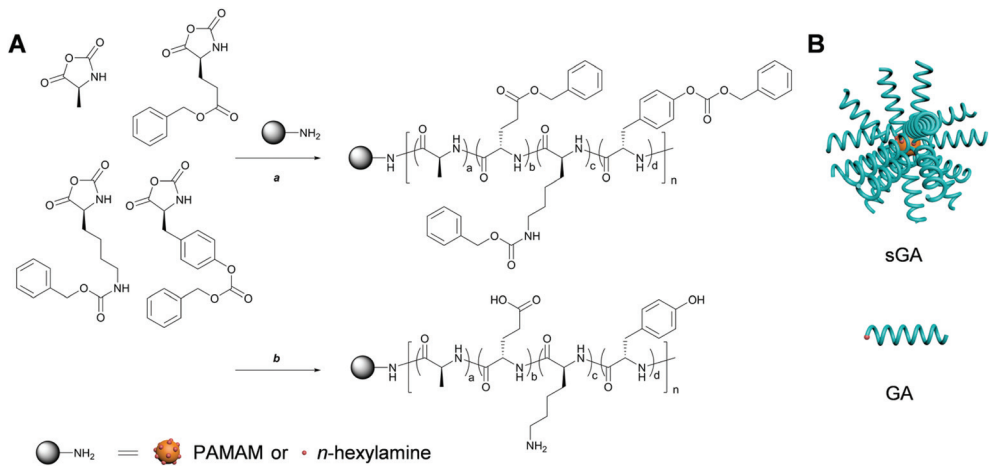

Scheme 1 Synthesis of sGA and GA. (A) Synthetic routes to sGA and GA. a DCM or DMF, room temperature, 2 h or overnight. b HBr, TFA, 0 °C, 1 h. (B) Schematic illustration of spherical, star-shaped sGA and linear GA.

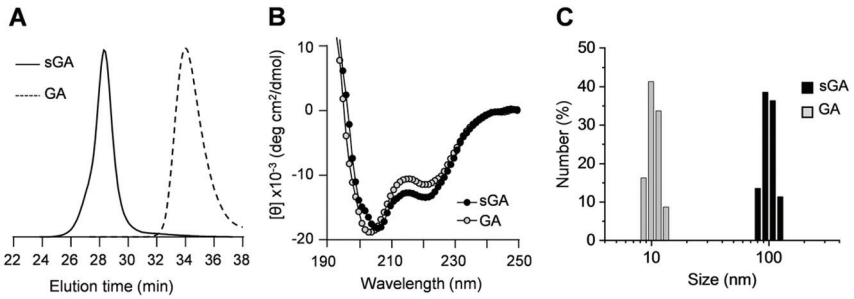

Fig. 1 Characterization of sGA and GA. (A) Normalized GPC-light scattering trace of polypeptide precursors of sGA and GA. (B) CD spectra of sGA and GA in an aqueous solution at pH = 7.0. (C) Number distribution of sGA and GA in an aqueous solution at pH = 7.0.

night using an *n*-hexylamine initiator (Scheme 1A). The resulting polypeptides were characterized by GPC, which revealed a monomodal MWD and indicated well-controlled polymerization (sGA precursor: M_n = 706 kDa, $Đ$ = 1.31; GA precursor: M_n = 15.1 kDa, $Đ$ = 1.09) (Fig. 1A). The fractions of incorporated amino acid residues were determined from the NMR spectrum to be 43.9% Ala, 33.9% Lys, 12.8% Glu, and 9.4% Tyr for sGA (Fig. S2A†), agreeing with the feeding NCA ratios (42.4% Ala, 34.0% Lys, 14.2% Glu, and 9.4% Tyr). Similarly, the fractions of amino acid residues were 41.9% Ala, 34.4% Lys, 15.0% Glu, and 8.7% Tyr for GA (Fig. S2B†), suggesting a composition similar to that of sGA. Finally, side-chain deprotection was achieved by treating the polypeptides with HBr, which efficiently removed >97% of the benzyloxycarbonyl protecting groups on BLG, ZLL, and BLT residues (Fig. S3†).

The aqueous solutions of sGA and GA exhibited similar traces and molecular ellipticity on CD spectra (Fig. 1B), suggesting that the change in the architecture showed minimal impact on the secondary structures of the polypeptides. The double-minimum curve at 205 and 222 nm was consistent with the previously reported spectra,[39] which was attributed to a mixture of α-helical and β-sheet conformations. Additionally, DLS analysis revealed that sGA (98.4 nm) was much larger in size than GA (10.7 nm) (Fig. 1C), in agreement with our polymer design and indicating the branched, star-shaped architecture of sGA (Scheme 1B).

3.2 Prolonged circulation of sGA compared to GA

To test our hypothesis that the change in polymer architecture alters its properties and function, we first compared the retention of branched sGA and linear GA in the body. We chose the i.p. route of administration, because i.p. injection of GA has shown similar or even better efficacy in ameliorating autoimmune diseases than s.c. injection,[40,41] and is equivalent to intravenous administration. Cy5-labelled GA and sGA were i.p. injected into adult mice, and systemic circulation of the polymers was evaluated by quantifying the fluorescence intensity in the blood. The fluorescently labelled polymers were prepared by reacting the lysine residues with the Cy5 NHS ester (Fig. S4A†). Due to the different labelling efficiencies of GA and sGA, different amounts of Cy5 NHS ester were added during the labelling reaction to ensure similar fluorescence intensities of GA and sGA at the same concentration (Fig. S4B†). At 0.5 h, sGA and GA showed similar concentrations in the blood. However, the plasma concentration of GA decreased rapidly, as the fluorescence signals became no

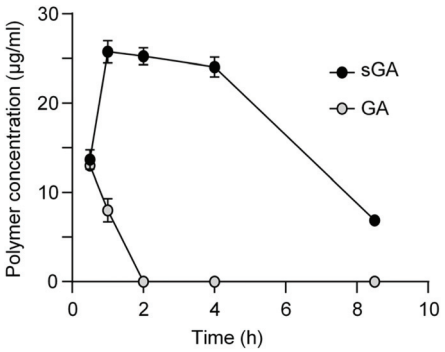

Fig. 2 *In vivo* pharmacokinetics (i.p. injection) of Cy5-labelled sGA and GA (n = 5).

longer detectable at 2 h (Fig. 2). In sharp contrast, the plasma concentration of sGA first increased 1 h after injection, and persisted at a concentration of around 25 μg mL^{-1} 4 h after injection (Fig. 2). Cy5-labelled sGA remained detectable in the blood 8 h post-injection (Fig. 2). These results indicate better hydrolytic stability of sGA compared with GA.

3.3 Rapid cell uptake of sGA by APCs *in vitro*

Recognition by immune cells is key in GA efficiency.[42] Cy5-labelled sGA or GA was used to visualize internalization of the polymeric drugs by APCs. Internalization of sGA into RAW 264.7 macrophages was visualized after a 60 min incubation, and exhibited higher fluorescence intensity than Cy5-labelled GA (Fig. 3A). Quantitative analysis of more than 100 cells per group revealed a significantly higher integrated density per cell of sGA than GA, with a clear time-dependent manner of polymer uptake (Fig. 3B). A similar experiment was conducted using BMDCs after 30 min incubation (Fig. 3C), which also revealed that APC internalization of sGA was superior to that of GA.

3.4 Enhanced therapeutic efficacy of sGA with a single low-dose treatment

The enhanced hydrolytic stability, prolonged tissue retention, and improved APC internalization of sGA provided us an impetus to further investigate its ability to reduce clinical scores during EAE disease in C57BL/6 mice. Surprisingly, one injection of sGA at 2 dpi at 10 mg kg^{-1} almost completely suppressed EAE symptoms (Fig. 4A). The average disease score of sGA-treated mice was below 0.5 (indicated by partial tail limpness) over the course of 27 dpi (Fig. 4A). On the other hand, two injections of GA (10 mg kg^{-1}) at 2 and 5 dpi did not show significant suppression of EAE symptoms (Fig. 4A). The AUC values, which are useful for quantifying EAE disease severity, were 27.4 ± 2.2, 0.75 ± 0.24, and 19.4 ± 2.5 for non-treated, sGA-treated, and GA-treated mice, respectively. While GA-treatment partially suppressed peak severity at around 18 to 21 dpi, disease severity between GA-treated and non-treated mice was not significantly different from 22 dpi onwards until mice were euthanized at 28 dpi. This result validates the frequent injection of GA (*i.e.*, daily or three-times-weekly) in previous studies, as double-dosing of GA is not able to suppress EAE symptoms.

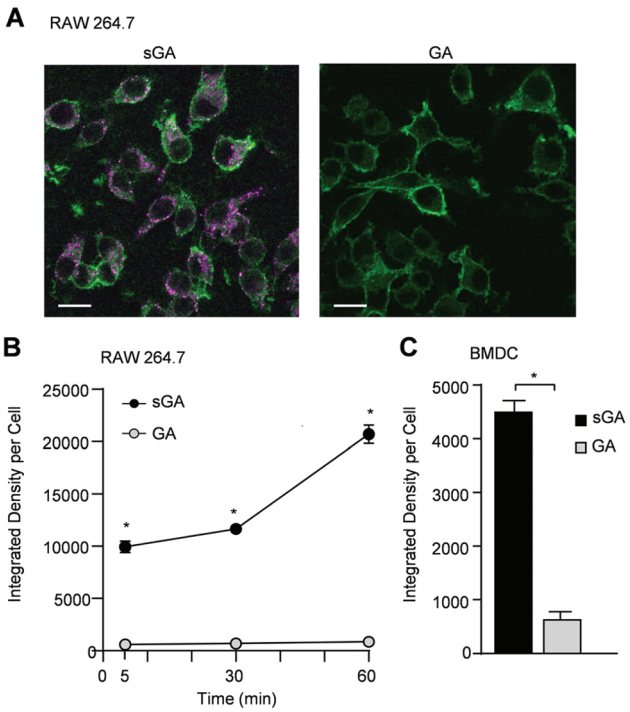

Fig. 3 *In vitro* cell uptake of sGA and GA by APCs. (A) Representative confocal images showing colocalization of Cy5-labelled sGA and GA (purple) with the cytoplasms of RAW 264.7 macrophages after 60 min treatment. The cells were stained with FITC-CD11b antibody (green). Scale bar = 10 μm. (B) Quantification of integrated density per RAW 264.7 cell after 5, 30, and 60 min treatment with Cy5-labelled sGA and GA. (C) Quantification of integrated density per BMDC after 30 min treatment with Cy5-labelled sGA and GA. *$p < 0.05$, two-tailed unpaired Student's t-test.

We further studied the dose-dependent efficacy of sGA in treating EAE. Decreasing the dosage of sGA by 10 fold (1 mg kg^{-1}) resulted in satisfactory suppression of EAE severity, as evidenced by the low AUC values observed until 27 dpi (Fig. 4B). Meanwhile, increasing the dosage of GA to 100 mg kg^{-1} improved the EAE scores, but still showed much higher AUC values than sGA treatment (Fig. 4B), further demonstrating the poor performance of GA at a significantly decreased injection frequency.

3.5 Reduced demyelination and T cell infiltration into the CNS after sGA treatment

MS and EAE are characterized by demyelination of neurons in the CNS. To verify whether sGA protected the myelin sheath from damage, spinal cord tissue sections at 28 dpi were stained with LFB. Consistent with their lack of EAE symptoms, sGA-treated mice had no reduction of LFB staining in the white matter of lumbar spinal cord when compared to non-treated EAE mice (Fig. 5A). On the other hand, GA-treated mice demonstrated reduction in LFB staining in spinal cord

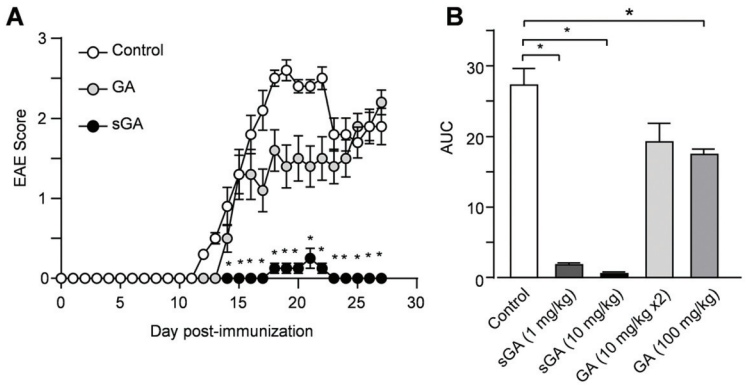

Fig. 4 *In vivo* therapeutic efficacy of sGA and GA treatment in EAE mice. (A) 6–8-week-old C57BL/6 mice were induced with EAE and treated with either sGA at 2 dpi (single injection, n = 4) or GA at 2 and 5 dpi (two injections, n = 5) at 10 mg kg^{-1}. The EAE behavioural score was monitored daily from 0 to 27 dpi for neurologic signs. *p < 0.05, two-tailed unpaired Student's t-test from 13 to 27 dpi. (B) AUC of clinical scores from 0 to 27 dpi for treatment conditions (single sGA injection at 1 mg kg^{-1}, single sGA injection at 10 mg kg^{-1}, two GA injections at 10 mg kg^{-1} each, and single GA injection at 100 mg kg^{-1}) was calculated. Statistical differences were calculated using Student's t-test (n = 4 to 8 per treatment group). Non-treated mice were used as negative controls. *p < 0.05, two-tailed unpaired Student's t-test.

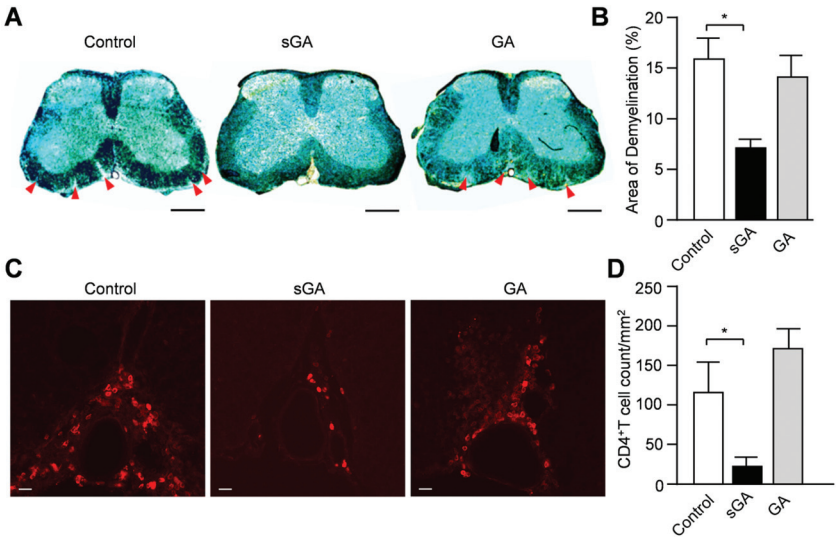

Fig. 5 Analysis of demyelination and CD4$^+$ T cell infiltration in spinal cord slices from mice euthanized at 28 dpi. (A) Representative brightfield images of LFB-stained lumbar spinal cord, with no treatment, sGA treatment, and GA treatment groups at 28 dpi. Scale bar = 500 μm. Red arrows indicate the demyelination area. (B) Quantification of spinal cord demyelination based on whole spinal cord slices. (C) Representative confocal images of ventral median fissure of OCT-embedded lumbar spinal cord with fluorescent CD4 staining from no treatment, sGA treatment, and GA treatment groups at 28 dpi. Scale bar = 20 μm. (D) Quantification of CD4$^+$ T cells from spinal cord sections as shown in (C). For (B) and (D), statistical differences were calculated using Student's t-test (n = 4 per treatment group). Non-treated mice were used as negative controls. *p < 0.05, two-tailed unpaired Student's t-test.

white matter, similar to control EAE condition (Fig. 5B). Demyelination in the CNS of EAE-induced mice is attributed to infiltration of peripheral CD4$^+$ T cells.[43] To examine if sGA influences immune cell infiltration into the CNS, tissue sections of spinal cord from GA- or sGA-treated EAE mice at 28 dpi were histologically processed and stained for CD4, which is expressed by and a marker of T helper cells. A total of 1615 cells (control: 742 cells; GA: 796 cells; and sGA: 72 cells) were included in our analyses by manual counting from a single blinded experimenter (Fig. 5C). CD4$^+$ T cell infiltration in the spinal cord was significantly reduced in the sGA condition compared with the GA condition (Fig. 5D). No difference in infiltrated CD4$^+$ T cell number was found between non-treated and GA-treated conditions. Together, these results indicate that sGA reduced infiltration of CD4$^+$ T cells to the spinal cord and prevented white matter demyelination.

4. Discussion

GA is one of the few synthetic polymeric therapeutics approved by US Food and Drug Administration and European Medicines

Agency. The intrinsic heterogeneity of random copolymers may cause some concerns in terms of therapeutic applications. However, recent developments in polymer chemistry, including the controlled polymerization technique, versatile side-chain design, and complex polymer architecture, offer a rich toolbox for researchers to further improve the performance of the macromolecular therapeutics. In this work, we present a unique way to enhance the therapeutic efficacy of synthetic polymers by altering their architecture. Specifically, advances in accelerated polymerization of NCA outpaces various side reactions that occur during the preparation of polypeptide materials, resulting in well-defined star-shaped GA with no obvious low-MW contaminates.

GA quickly hydrolyses into lower-MW fragments at the injection site within 1 h,[18,19] and is also rapidly degraded in the plasma after i.p. injection. In contrast, sGA showed significantly enhanced retention and slower degradation than linear GA. This result is in agreement with previous studies on star-shaped polypeptides.[27] The enhanced stability of sGA is presumably attributed to its branched structure with densely packed arms, which blocks enzyme access and slows down the degradation of the polypeptide backbones. Because of the slower degradation and longer retention of sGA, we speculated that less frequent injections or low doses of sGA would achieve similar efficacy as frequent injection and high dose of GA. In fact, while two injections of high-dose (10 mg kg^{-1}) GA cannot suppress EAE disease significantly, a single injection of a low dose (1 mg kg^{-1}) of sGA is sufficient to strongly suppress EAE symptoms. Interestingly, although sGA was administered to animals at EAE 2 dpi, its effect on disease suppression was apparent through around 30 dpi. This efficacy resembles that of a recently reported GA deport requiring fewer injections, which showed sustained, 30-day release of GA from microspheres.[44] It is tempting to speculate that therapeutic efficacy of low dose sGA can be further improved if delivered *via* highly efficient and controllable drug-carrying vehicles.[45–47] In addition to improvements in hydrolytic stability and prolonged tissue retention of sGA, its enhanced performance in suppressing EAE symptoms may be directly attributed to its interaction with immune cells such as APCs, which are crucial players in autoimmunity. In fact, it has been reported before that nanoparticles with a high surface density of ligands produce more profound changes in APC effector function.[48]

GA has been shown to modulate APC effector function by competing against pathogenic myelin-specific peptides in the process of antigen presentation. GA can bind directly to class II major histocompatibility complex (MHC) molecules on cell surface of APC thus limiting the presentation of other antigen peptides;[49] alternatively, GA has also been shown to penetrate into intracellular spaces to be further processed for antigen presentation or even influence intracellular signalling pathways.[50] This outcome may be explained by the multivalent effect.[24,51,52] Notably, *in vitro* RAW264.7 macrophage and BMDC cell uptake of sGA is rapid, highlighting the their affinity for cell attachment and uptake. sGA internalization by APCs may be facilitated by active cellular endocytosis[53] or an energy-independent process of cell entry by polypeptide-mediated pore formation.[24]

Upon cellular entry, sGA is expected to be cleaved from its core, resulting in the release of functional peptides within the cell. Once inside a cell, antigenic peptides can undergo endosomal processing for antigen presentation to be presented by class II MHC molecules on membrane surface.[54,55] In fact, GA was previously shown to be rapidly internalized by B cells, another group of APCs, then presented on cell surface by MHC II molecule.[50] Therefore, in addition to longer bodily retention, we speculate that the improvement in surface-binding and polymer internalization kinetics seen in sGA at cellular level allows it to more strongly compete against MOG peptide presentation and suppress EAE severity, thereby resulting in significant disease amelioration as evidenced by reduced motor dysfunction, demyelination, and $CD4^+$ T infiltration into spinal cord. In addition to regulating APC antigen presentation behaviour, sGA may enhance anti-inflammatory cytokine production, decrease pro-inflammatory cytokine production,[56,57] and exert its effects directly on T cells,[58] which are reported as GA function.

Overall, the work described here demonstrates that the power of advances in polymer design in improving the efficacy of an established, widely used polymeric therapeutic. In order to further evaluate the potentials of sGA as an effective treatment for MS, the therapeutic efficacy of sGA will be compared with commercially available GA in our future studies. Additionally, the safety profile and the performance of sGA through s.c. injection will be conducted, which provide essential information for the future applications of sGA.

5. Conclusion

In summary, we report the development of a branched, star-shaped polypeptide, sGA, which exhibits therapeutic efficacy in treating EAE disease that is superior to that of regular, linear GA. Due to its improved degradation/retention profile as well as its enhanced APC interactions, sGA shows a satisfactory effect on suppressing EAE symptoms even with one injection at a low dose. In addition, significantly less demyelination and T cell infiltration of the spinal cord were observed in sGA-treated mice. The use of a lower dosage of sGA, together with less-frequent injections, greatly decreases preparation costs, providing a promising and economic candidate to treat MS. This work also presents an interesting way to improve efficacy through the structural control of polymers, which may shed light on the future development of synthetic polymeric therapeutics.

Conflicts of interest

There are no conflicts of interest to declare.

Acknowledgements

We acknowledge the support from National Science Foundation (CHE-1709820, J. C.), University of Illinois start-up funds (M. I.), and National Institutes of Health (R01-AI136999, M. I.). We thank C. Leal and L. Zheng for the access to the microplate reader.

References

1 A. J. Thompson, S. E. Baranzini, J. Geurts, B. Hemmer and O. Ciccarelli, Multiple sclerosis, *Lancet*, 2018, **391**, 1622–1636.
2 M. Filippi, A. Bar-Or, F. Piehl, P. Preziosa, A. Solari, S. Vukusic and M. A. Rocca, Multiple sclerosis, *Nat. Rev. Dis. Primers*, 2018, **4**, 43.
3 D. S. Reich, C. F. Lucchinetti and P. A. Calabresi, Multiple sclerosis, *N. Engl. J. Med.*, 2018, **378**, 169–180.
4 M. T. Wallin, W. J. Culpepper, E. Nichols, Z. A. Bhutta, T. T. Gebrehiwot, S. I. Hay, I. A. Khalil, K. J. Krohn, X. Liang, M. Naghavi, A. H. Mokdad, M. R. Nixon, R. C. Reiner, B. Sartorius, M. Smith, R. Topor-Madry, A. Werdecker, T. Vos, V. L. Feigin and C. J. L. Murray, Global, regional, and national burden of multiple sclerosis 1990–2016: a systematic analysis for the Global Burden of Disease Study 2016, *Lancet Neurol.*, 2019, **18**, 269–285.
5 M. Tintore, A. Vidal-Jordana and J. Sastre-Garriga, Treatment of multiple sclerosis - success from bench to bedside, *Nat. Rev. Neurosci.*, 2019, **15**, 53–58.
6 B. Weinstock-Guttman, K. V. Nair, J. L. Glajch, T. C. Ganguly and D. Kantor, Two decades of glatiramer acetate: From initial discovery to the current development of generics, *J. Neurol. Sci.*, 2017, **376**, 255–259.
7 D. Teitelbaum, A. Meshorer, T. Hirshfeld, R. Arnon and M. Sela, Suppression of experimental allergic encephalomyelitis by a synthetic polypeptide, *Eur. J. Immunol.*, 1971, **1**, 242–248.
8 C. Bell, J. Anderson, T. Ganguly, J. Prescott, I. Capila, J. C. Lansing, R. Sachleben, M. Iyer, I. Fier, J. Roach, K. Storey, P. Miller, S. Hall, D. Kantor, B. M. Greenberg, K. Nair and J. Glajch, Development of Glatopa® (glatiramer acetate): The first FDA-approved generic disease-modifying therapy for relapsing forms of multiple sclerosis, *J. Pharm. Pract.*, 2017, **31**, 481–488.
9 W. Schrempf and T. Ziemssen, Glatiramer acetate: Mechanisms of action in multiple sclerosis, *Autoimmun. Rev.*, 2007, **6**, 469–475.
10 M. B. Bornstein, A. Miller, S. Slagle, M. Weitzman, H. Crystal, E. Drexler, M. Keilson, A. Merriam, S. Wassertheil-Smoller, V. Spada, W. Weiss, R. Arnon, I. Jacobsohn, D. Teitelbaum and M. Sela, A pilot trial of Cop 1 in exacerbating–remitting multiple sclerosis, *N. Engl. J. Med.*, 1987, **317**, 408–414.
11 K. P. Johnson, B. R. Brooks, J. A. Cohen, C. C. Ford, J. Goldstein, R. P. Lisak, L. W. Myers, H. S. Panitch, J. W. Rose, R. B. Schiffer, T. Vollmer, L. P. Weiner and J. S. Wolinsky, Copolymer 1 reduces relapse rate and improves disability in relapsing-remitting multiple sclerosis: results of a phase III multicenter, double-blind, placebo-controlled trial, *Neurology*, 1995, **45**, 1268–1276.
12 G. Comi, M. Filippi, J. S. Wolinsky and European/Canadian Glatiramer Acetate Study Group, European/Canadian multicenter, double-blind, randomized, placebo-controlled study of the effects of glatiramer acetate on magnetic resonance imaging–measured disease activity and burden in patients with relapsing multiple sclerosis, *Ann. Neurol.*, 2001, **49**, 290–297.
13 J. Cohen, A. Belova, K. Selmaj, C. Wolf, M. P. Sormani, J. Oberyé, E. van den Tweel, R. Mulder, N. Koper, G. Voortman and F. Barkhof, Equivalence of generic glatiramer acetate in multiple sclerosis: A randomized clinical trial, *JAMA Neurol.*, 2015, **72**, 1433–1441.
14 M. Caporro, G. Disanto, C. Gobbi and C. Zecca, Two decades of subcutaneous glatiramer acetate injection: current role of the standard dose, and new high-dose low-frequency glatiramer acetate in relapsing-remitting multiple sclerosis treatment, *Patient Prefer. Adherence*, 2014, **8**, 1123–1134.
15 K. Hellwig, O. Neudorfer, S. Melamed-Gal, P. Baruch and S. Qassem, Pregnancy outcomes in patients with multiple sclerosis and exposure to branded glatiramer acetate during all three trimesters (P4.362), *Neurology*, 2018, **90**, P4.362.
16 O. Khan, P. Rieckmann, A. Boyko, K. Selmaj, R. Zivadinov and GALA Study Group, Three times weekly glatiramer acetate in relapsing–remitting multiple sclerosis, *Ann. Neurol.*, 2013, **73**, 705–713.
17 G. Cutter, A. Veneziano, A. Grinspan, M. Al-Banna, A. Boyko, M. Zakharova, E. Maida, M. B. Pasic, S. K. Gandhi, R. Everts, C. Cordioli and S. Rossi, Higher satisfaction and adherence with glatiramer acetate 40 mg/mL TIW vs 20 mg/mL QD in RRMS, *Mult. Scler. Relat. Disord.*, 2019, **33**, 13–21.
18 O. Neuhaus, B. C. Kieseier and H.-P. Hartung, Pharmacokinetics and pharmacodynamics of the interferon-betas, glatiramer acetate, and mitoxantrone in multiple sclerosis, *J. Neurol. Sci.*, 2007, **259**, 27–37.
19 S. Messina and F. Patti, The pharmacokinetics of glatiramer acetate for multiple sclerosis treatment, *Expert Opin. Drug Metab. Toxicol.*, 2013, **9**, 1349–1359.
20 W. Jiang, X. Xiao, Y. Wu, W. Zhang, Z. Cong, J. Liu, S. Chen, H. Zhang, J. Xie, S. Deng, M. Chen, Y. Wang, X. Shao, Y. Dai, Y. Sun, J. Fei and R. Liu, Peptide polymer displaying potent activity against clinically isolated multidrug resistant Pseudomonas aeruginosa in vitro and in vivo, *Biomater. Sci.*, 2020, **8**, 739–745.
21 E. Ben-Akiva, S. Est Witte, R. A. Meyer, K. R. Rhodes and J. J. Green, Polymeric micro- and nanoparticles for immune modulation, *Biomater. Sci.*, 2019, **7**, 14–30.
22 L. I. F. Moura, A. Malfanti, C. Peres, A. I. Matos, E. Guegain, V. Sainz, M. Zloh, M. J. Vicent and

H. F. Florindo, Functionalized branched polymers: promising immunomodulatory tools for the treatment of cancer and immune disorders, *Mater. Horiz.*, 2019, **6**, 1956–1973.
23 Z. Song, Z. Tan and J. Cheng, Recent advances and future perspectives of synthetic polypeptides from *N*-carboxyanhydrides, *Macromolecules*, 2019, **52**, 8521–8539.
24 L. Yin, Z. Song, K. H. Kim, N. Zheng, H. Tang, H. Lu, N. Gabrielson and J. Cheng, Reconfiguring the architectures of cationic helical polypeptides to control non-viral gene delivery, *Biomaterials*, 2013, **34**, 2340–2349.
25 Z. Kadlecova, Y. Rajendra, M. Matasci, L. Baldi, D. L. Hacker, F. M. Wurm and H.-A. Klok, DNA delivery with hyperbranched polylysine: a comparative study with linear and dendritic polylysine, *J. Controlled Release*, 2013, **169**, 276–288.
26 M. Byrne, D. Victory, A. Hibbitts, M. Lanigan, A. Heise and S.-A. Cryan, Molecular weight and architectural dependence of well-defined star-shaped poly(lysine) as a gene delivery vector, *Biomater. Sci.*, 2013, **1**, 1223–1234.
27 A. Duro-Castano, R. M. England, D. Razola, E. Romero, M. Oteo-Vives, M. A. Morcillo and M. J. Vicent, Well-defined star-shaped polyglutamates with improved pharmacokinetic profiles as excellent candidates for biomedical applications, *Mol. Pharm.*, 2015, **12**, 3639–3649.
28 R. Baumgartner, H. Fu, Z. Song, Y. Lin and J. Cheng, Cooperative polymerization of α-helices induced by macromolecular architecture, *Nat. Chem.*, 2017, **9**, 614–622.
29 H. Lu and J. Cheng, Hexamethyldisilazane-mediated controlled polymerization of α-amino acid *N*-carboxyanhydrides, *J. Am. Chem. Soc.*, 2007, **129**, 14114–14115.
30 J. R. Kramer, B. Onoa, C. Bustamante and C. R. Bertozzi, Chemically tunable mucin chimeras assembled on living cells, *Proc. Natl. Acad. Sci. U. S. A.*, 2015, **112**, 12574–12579.
31 A. J. Adler, N. J. Greenfield and G. D. Fasman, in *Methods Enzymol*, ed. C. H. W. Hirs and S. N. Timasheff, Academic Press, 1973, vol. 27, pp. 675–735.
32 N. J. Greenfield, Using circular dichroism spectra to estimate protein secondary structure, *Nat. Protoc.*, 2006, **1**, 2876–2890.
33 G. Polymeropoulos, G. Zapsas, K. Ntetsikas, P. Bilalis, Y. Gnanou and N. Hadjichristidis, 50th anniversary perspective: polymers with complex architectures, *Macromolecules*, 2017, **50**, 1253–1290.
34 J. M. Ren, T. G. McKenzie, Q. Fu, E. H. H. Wong, J. Xu, Z. An, S. Shanmugam, T. P. Davis, C. Boyer and G. G. Qiao, Star polymers, *Chem. Rev.*, 2016, **116**, 6743–6836.
35 J.-F. Lutz, J.-M. Lehn, E. W. Meijer and K. Matyjaszewski, From precision polymers to complex materials and systems, *Nat. Rev. Mater.*, 2016, **1**, 16024.
36 X. Wang, Z. Song, Z. Tan, L. Zhu, T. Xue, S. Lv, Z. Fu, X. Zheng, J. Ren and J. Cheng, Facile synthesis of helical multiblock copolypeptides: minimal side reactions with accelerated polymerization of N-carboxyanhydrides, *ACS Macro Lett.*, 2019, **8**, 1517–1521.
37 Z. Song, H. Fu, J. Wang, J. Hui, T. Xue, L. A. Pacheco, H. Yan, R. Baumgartner, Z. Wang, Y. Xia, X. Wang, L. Yin, C. Chen, J. Rodríguez-López, A. L. Ferguson, Y. Lin and J. Cheng, Synthesis of polypeptides via bioinspired polymerization of in situ purified *N*-carboxyanhydrides, *Proc. Natl. Acad. Sci. U. S. A.*, 2019, **116**, 10658–10663.
38 S. Lv, H. Kim, Z. Song, L. Feng, Y. Yang, R. Baumgartner, K.-Y. Tseng, S. J. Dillon, C. Leal, L. Yin and J. Cheng, Unimolecular polypeptide micelles via ultra-fast polymerization of *N*-carboxyanhydrides, *J. Am. Chem. Soc.*, 2020, **142**, 8570–8574.
39 R. Stapulionis, C. L. P. Oliveira, M. C. Gjelstrup, J. S. Pedersen, M. E. Hokland, S. V. Hoffmann, K. Poulsen, C. Jacobsen and T. Vorup-Jensen, Structural insight into the function of myelin basic protein as a ligand for integrin $\alpha_M\beta_2$, *J. Immunol.*, 2008, **180**, 3946–3956.
40 R. Aronovich, A. Katzav and J. Chapman, The strategies used for treatment of experimental autoimmune neuritis (EAN): A beneficial effect of glatiramer acetate administered intraperitoneally, *Clin. Rev. Allergy Immunol.*, 2012, **42**, 181–188.
41 S. Bittner, T. Ruck, K. Göbel, C. Henschel, A. M. Afzali, E. Göb, T. Müntefering, C. Kleinschnitz, H. Wiendl and S. G. Meuth, Effects of glatiramer acetate in a spontaneous model of autoimmune neuroinflammation, *Am. J. Pathol.*, 2014, **184**, 2056–2065.
42 P. H. Lalive, O. Neuhaus, M. Benkhoucha, D. Burger, R. Hohlfeld, S. S. Zamvil and M. S. Weber, Glatiramer acetate in the treatment of multiple sclerosis, *CNS Drugs*, 2011, **25**, 401–414.
43 S. Desplat-Jégo, R. Creidy, S. Varriale, N. Allaire, Y. Luo, D. Bernard, K. Hahm, L. Burkly and J. Boucraut, Anti-TWEAK monoclonal antibodies reduce immune cell infiltration in the central nervous system and severity of experimental autoimmune encephalomyelitis, *Clin. Immunol.*, 2005, **117**, 15–23.
44 A. Miller, L. Popper, U. Danon, N. B. Kimelman, S. Rubnov, E. Marom, J. Chapman, A. Shifrin, R. Gilad, D. Karussis, R. Milo, C. Hoffmann, S. Flechter and A. Karni, Glatiramer acetate depot (extended-release) Phase IIa one-year study in patients with relapsing-remitting multiple sclerosis: safety, tolerability and efficacy – NEDA analysis (P6.359), *Neurology*, 2018, **90**, P6.359.
45 X. Gu, M. Qiu, H. Sun, J. Zhang, L. Cheng, C. Deng and Z. Zhong, Polytyrosine nanoparticles enable ultra-high loading of doxorubicin and rapid enzyme-responsive drug release, *Biomater. Sci.*, 2018, **6**, 1526–1534.
46 Y. Wu, S. Lv, Y. Li, H. He, Y. Ji, M. Zheng, Y. Liu and L. Yin, Co-delivery of dual chemo-drugs with precisely controlled, high drug loading polymeric micelles for synergistic anticancer therapy, *Biomater. Sci.*, 2020, **8**, 949–959.
47 Y. Zhong, F. Meng, W. Zhang, B. Li, J. C. M. van Hest and Z. Zhong, CD44-targeted vesicles encapsulating granzyme B as artificial killer cells for potent inhibition of human multiple myeloma in mice, *J. Controlled Release*, 2020, **320**, 421–430.
48 A. Bandyopadhyay, R. L. Fine, S. Demento, L. K. Bockenstedt and T. M. Fahmy, The impact of nano-

particle ligand density on dendritic-cell targeted vaccines, *Biomaterials*, 2011, **32**, 3094–3105.

49 M. Kala, S. N. Rhodes, W.-H. Piao, F.-D. Shi, D. I. Campagnolo and T. L. Vollmer, B cells from glatiramer acetate-treated mice suppress experimental autoimmune encephalomyelitis, *Exp. Neurol.*, 2010, **221**, 136–145.

50 L. J. Jackson, S. Selva, T. L. Niedzielko and T. Vollmer, B cell receptor recognition of glatiramer acetate is required for efficacy through antigen presentation and cytokine production, *J. Clin. Cell. Immunol.*, 2014, **5**, 1–14.

51 K. E. B. Doncom, L. D. Blackman, D. B. Wright, M. I. Gibson and R. K. O'Reilly, Dispersity effects in polymer self-assemblies: a matter of hierarchical control, *Chem. Soc. Rev.*, 2017, **46**, 4119–4134.

52 A. B. Cook and S. Perrier, Branched and dendritic polymer architectures: Functional nanomaterials for therapeutic delivery, *Adv. Funct. Mater.*, 2020, **30**, 1901001.

53 M. E. C. Lutsiak, D. R. Robinson, C. Coester, G. S. Kwon and J. Samuel, Analysis of poly(D,L-lactic-co-glycolic acid) nanosphere uptake by human dendritic cells and macrophages *in vitro*, *Pharm. Res.*, 2002, **19**, 1480–1487.

54 K. Mahnke, M. Guo, S. Lee, H. Sepulveda, S. L. Swain, M. Nussenzweig and R. M. Steinman, The dendritic cell receptor for endocytosis, Dec-205, can recycle and enhance antigen presentation via major histocompatibility complex class II–positive lysosomal compartments, *J. Cell Biol.*, 2000, **151**, 673–684.

55 S. Burgdorf, A. Kautz, V. Böhnert, P. A. Knolle and C. Kurts, Distinct pathways of antigen uptake and intracellular routing in CD4 and CD8 T cell activation, *Science*, 2007, **316**, 612–616.

56 R. Carpintero, K. J. Brandt, L. Gruaz, N. Molnarfi, P. H. Lalive and D. Burger, Glatiramer acetate triggers PI3Kδ/Akt and MEK/ERK pathways to induce IL-1 receptor antagonist in human monocytes, *Proc. Natl. Acad. Sci. U. S. A.*, 2010, **107**, 17692.

57 N. Molnarfi, T. Prod'homme, U. Schulze-Topphoff, C. M. Spencer, M. S. Weber, J. C. Patarroyo, P. H. Lalive and S. S. Zamvil, Glatiramer acetate treatment negatively regulates type I interferon signaling, *Neurol. Neuroimmunol. Neuroinflamm.*, 2015, **2**, e179.

58 R. Aharoni, D. Teitelbaum, R. Arnon and M. Sela, Copolymer 1 acts against the immunodominant epitope 82–100 of myelin basic protein by T cell receptor antagonism in addition to major histocompatibility complex blocking, *Proc. Natl. Acad. Sci. U. S. A.*, 1999, **96**, 634–639.